Title
On the sizes and lifetimes of cold pools

Journal
Quarterly Journal of the Royal Meteorological Society, 142(696)

ISSN
0035-9009

Authors
Romps, David M
Jeevanjee, Nadir

Publication Date
2016-04-01

DOI
10.1002/qj.2754

Peer reviewed

On the sizes and lifetimes of cold pools

David M. Romps

Nadir Jeevanjee
First published: 29 January 2016
https://doi.org/10.1002/qj.2754
Cited by: 1
UC-eLinks

Abstract

Cold pools of air, which are formed by evaporating precipitation, play a critical role in the triggering of new precipitation. Despite their recognized importance, little effort has been devoted to building simple models of their dynamics. Here, analytical equations are derived for the radius, height, and buoyancy of a cylindrical cold pool as a function of time, and a scale analysis reveals that entrainment is a dominant influence. These governing equations yield simple expressions for the maximum sizes and lifetimes of cold pools. The terminal radius of a cold pool is relatively insensitive to its initial conditions, with a typical maximum radius of about 14 times the initial radius, give or take a factor of 2. The terminal time of a cold pool, on the other hand, can vary over orders of magnitude depending on its initial potential and kinetic energies. These predictions are validated against large-eddy simulations.

1 Introduction

By evaporative cooling, convective precipitation can generate cold patches of boundary-layer air. These negatively buoyant air masses spread out radially, forming ‘cold pools’ that push up other boundary-layer air at their edge and thereby trigger new convection. In particular, cold pools are responsible for triggering boundary-layer updraughts that are wide enough to convect deeply and precipitate (Khairoutdinov and Randall, 2006; Böing *et al.*, 2012), leading to a chain reaction of deep convection, precipitation, cold pools, deep convection, and so on. Since cold pools trigger new updraughts by mechanical forcing (Torri *et al.*, 2015; Jeevanjee and Romps, 2015), understanding cold-pool dynamics is one of the keys to understanding tropical precipitation.

In this article, we develop an ‘integral’ or ‘box’ model of a uniform, cylindrical cold pool. Such models have been used with some success to study gravity currents in a wide range of applications (Huppert and Simpson, 1980; Dade and Huppert, 1995; Huppert, 1998; Harris *et al.*, 2001; Ross *et al.*, 2004; Hogg *et al.*, 2005). Here, we develop the governing equations for a cold pool that is subject to entrainment, form drag, and surface fluxes of enthalpy and momentum. With these governing equations, we aim to develop a theory for the sizes and lifetimes of cold pools in the tropical atmosphere. Such a theory would be particularly relevant to global climate models, many of which have begun to include representations of cold pools in their convective parametrizations (Qian *et al.*, 1998; Rozbicki *et al.*, 1999; Grandpeix *et al.*, 2009; Grandpeix and Lafore, 2010; Rio *et al.*, 2013; Del Genio *et al.*, 2015).

2 Cylindrical cold pool

Consider a cylindrical cold pool that is characterized by a radius R, height H, uniform density anomaly ρ' (relative to the environmental air at the same height), and a radial velocity u^r that is independent of z and proportional to the radial coordinate r. Let us denote the volume of a cold pool by V, which is related to R and H by

(1) $$V = \pi H R^2 .$$

We will denote the rate of change of the cold pool's radius as $U \equiv \mathrm{d}R/\mathrm{d}t$. Within the cold pool, the radial velocity u^r will be defined as

(2). $$u^r = \frac{U}{R} r .$$

By continuity,

(3). $$w = -\frac{2U}{R} z .$$

Therefore, the total kinetic energy of the cold pool is

(4). $$w = -\frac{2U}{R} z .$$

For $R \gg H$, the specific kinetic energy is simply $U^2/4$. The gravitational potential energy of the cold pool is simply

(5) $$\mathrm{PE} = \frac{g\rho' VH}{2} .$$

Changes in volume occur through entrainment. We write this as

$$\frac{\mathrm{d}}{\mathrm{d}t}V = \varepsilon U V, \tag{6}$$

where ε, which has units of m^{-1}, is the fractional entrainment per distance traveled by the cold pool's front. For example, if a cold pool has a volume of 1 km^3 and an entrainment rate of $\varepsilon = 10^{-4}$ m^{-1}, then it will entrain 10^5 m^3 as its radius increases by one metre. By entraining environmental air with zero density anomaly, entrainment tends to reduce the cold pool's density anomaly according to the following equation:

$$\left(\frac{\mathrm{d}}{\mathrm{d}t}\rho'\right)_{\text{entrainment}} = -\varepsilon U \rho'. \tag{7}$$

3 Sinks of energy

Our goal is to obtain a set of governing equations for the cold pool, including an equation for dU/dt. The gravity-current box models constructed by Huppert and Simpson (1980), Ross *et al.* (2004), and many others have neglected cold-pool dynamics entirely. Instead, those studies have assumed that the cold pool's front moves at a speed U that is proportional to $\sqrt{Hg\rho'/\rho}$; this is equivalent to assuming that the Froude number $U/\sqrt{Hg\rho'/\rho}$ is constant. This is a poor assumption because, in reality, the Froude number starts at zero (for an initially stationary cold pool), grows to positive values (as U grows), goes to infinity (as ρ' goes to zero), and then becomes imaginary (for negative ρ'). In this study, all of the large-eddy simulations (LES) of cold pools with surface enthalpy fluxes exhibit this behaviour, regardless of whether H and ρ' are calculated for the entire cold pool or just its head. Clearly, the assumption of a constant Froude number is inadequate for modelling cold-pool dynamics.

We will find the governing equation for U by constructing the budget for the cold pool's total energy TE, which is the sum of its potential energy PE and its kinetic energy KE. If we can determine the sources and sinks of TE, then we can write down the energy equation, which will take the form

$$\frac{\mathrm{d}}{\mathrm{d}t}\mathrm{TE} \equiv \frac{\mathrm{d}}{\mathrm{d}t}(\mathrm{KE}+\mathrm{PE}) = \text{sinks}. \tag{8}$$

Only one dU/dt will appear in this equation, and it is generated by d/dt acting on U^2 in the definition of KE. By rearranging, this will give us our prognostic governing equation for U.

There are five sinks of total energy, which are caused by entrainment, surface drag, form drag, other pressure forces, and surface enthalpy fluxes. These five sinks are described in the following subsections.

3.1 *Entrainment*

Entrainment reduces kinetic energy by diluting the momentum. Consider a parcel with mass $m$and speed u. Its momentum is mu and its kinetic energy KE is $mu^2/2$. If the parcel entrains a mass dm with no momentum, then its mass goes to m + dm by conservation of mass and its speed goes to $mu/(m + \mathrm{d}m)$ by conservation of momentum. Therefore, KE goes to (1 − dm/m)KE. By analogy, when the cold pool entrains a mass fraction $\varepsilon U\mathrm{d}t$, we will assume that the cold pool's KE goes to (1 − $\varepsilon U\mathrm{d}t$)KE. Therefore, entrainment affects total energy by

$$\left(\frac{\mathrm{d}}{\mathrm{d}t}\mathrm{TE}\right)_{\text{entrainment}} = -\varepsilon U\mathrm{KE}. \tag{9}$$

Note that entrainment will also ‘puff up’ the cold pool, leading to a lifting of the centre of mass of ρ' and, as a result, an increase in PE. We assume, however, that this increase in PE is obtained at the expense of KE, so that this has no net effect on the total energy. (Note that turbulent entrainment can only occur if there is motion, i.e. positive KE, so this effect will never drive KE to negative values.)

3.2 *Surface drag*

Surface drag reduces kinetic energy by operating on the cold pool with a force opposite to its motion. Using a bulk formula for the surface momentum flux, surface drag reduces total energy according to

$$\left(\frac{\mathrm{d}}{\mathrm{d}t}\mathrm{TE}\right)_{\text{surface drag}} = -\int_A c_{\mathrm{ds}}\rho u'^3\,\mathrm{d}^2x = -\frac{2}{5}\pi c_{\mathrm{ds}}\rho R^2 U^3\,, \tag{10}$$

(10).

where A is the area underneath the cold pool and c_{ds}=1.5 × 10^{-3} is the surface drag coefficient.

3.3 *Form drag*

Form drag, caused by pressure forces between the cold pool and the environment, also reduces kinetic energy. Dissipation of energy from form drag is given by the integral of $c_{df}\rho U^3/2$ over the cold pool's outer boundary area $2\pi RH$, where c_{df} is the form drag coefficient. This gives

(11)

$$\left(\frac{\mathrm{d}}{\mathrm{d}t}\mathrm{TE}\right)_{\text{form drag}} = -\pi c_{\mathrm{df}}\rho R H U^3\,.$$

The correct value for c_{df} is unknown. It will be treated as a tunable parameter and found by optimization.

3.4 *Other pressure forces*

Form drag is not the only force acting between the cold pool and its environment. There are other pressure-gradient forces that cannot be written with the standard drag-law formulation used in Eq. 11. For example, a completely stationary cold pool will have, in addition to the standard definition of buoyancy, additional pressure-gradient forces acting between it and its environment. These forces act to accelerate the environment so that the boundaries of the cold pool may move without violating the continuity equation and they cause the cold pool to accelerate less rapidly than would be estimated from buoyancy alone. The ‘effective buoyancy’ (Davies-Jones, 2003), which gives the net vertical acceleration due to density gradients, is particularly useful for understanding this process. Jeevanjee and Romps (2016) have calculated analytical expressions for effective buoyancy and have found that, for air at the surface, the difference between buoyancy and effective buoyancy is particularly pronounced: for a cylindrical cold pool at the surface with H = R, the effective buoyancy is only about a quarter that of the buoyancy. This does not mean, however, that only a quarter of the cold pool's initial PE is converted to the cold pool's KE. Instead, the cold pool treats the overlying environment like a flywheel, pumping energy into it initially only to extract much of that energy as the cold pool is squashed by the descending environment. Rather than attempt to model this complicated dynamics in any detail, we will simply define α as the fraction of the cold pool's initial potential energy that is immediately or eventually converted to kinetic energy of the cold pool; $1 - \alpha$ is the fraction that is permanently lost to the environment by pressure forces not attributable to form drag. Rather than write this as an explicit sink, we will simply introduce a factor of α in the definition of the cold pool's potential energy PE, modifying Eq. 5 to

(12).

$$\mathrm{PE} = \frac{\alpha g \rho' V H}{2} .$$

The correct value for α is unknown, other than the fact that it must be between zero and one. Like c_{df}, its value will be found by optimization.

3.5 *Surface enthalpy fluxes*

Surface enthalpy fluxes reduce the density anomaly ρ' and therefore the potential energy. For surface fluxes of the density anomaly, we can write

$$\begin{aligned} \left(\frac{\mathrm{d}}{\mathrm{d}t}\rho'\right)_{\text{surface fluxes}} &= \frac{1}{V}\int_A c_{\mathrm{ds}} u^{r}(\rho'_{\mathrm{s}} - \rho')\,\mathrm{d}^2x \\ &= -\frac{2}{3}c_{\mathrm{ds}}\left(1 - \frac{\rho'_{\mathrm{s}}}{\rho'}\right)\frac{U}{H}\rho' , \end{aligned} \quad (13)$$

where ρ'_{s} is the density of air that would be in equilibrium with the surface. Since PE is proportional to ρ', these surface enthalpy fluxes reduce TE according to

$$\left(\frac{\mathrm{d}}{\mathrm{d}t}\mathrm{TE}\right)_{\text{surface fluxes}} = -\frac{2}{3}c_{\mathrm{ds}}\left(1 - \frac{\rho'_{\mathrm{s}}}{\rho'}\right)\frac{U}{H}\mathrm{PE} . \quad (14)$$

4 Governing equations

We can now specify the right-hand side of Eq. 8 as the sum of all of the sinks given by Eqs 9, 10, 11, and 14. This gives

$$\frac{\mathrm{d}}{\mathrm{d}t}\mathrm{KE} + \frac{\mathrm{d}}{\mathrm{d}t}\mathrm{PE} = -\varepsilon U\mathrm{KE} - \frac{2}{5}\pi c_{\mathrm{ds}}\rho R^2 U^3 - \pi c_{\mathrm{df}}\rho RHU^3 - \frac{2}{3}c_{\mathrm{ds}}\left(1 - \frac{\rho_{\mathrm{s}}'}{\rho'}\right)\frac{U}{H}\mathrm{PE}\,. \qquad (15)$$

Next, we need to write dPE/dt and dKE/dt in terms of U and dU/dt. For dPE/dt, we first need to get an expression for the total time derivative of ρ', which we obtain by combining Eqs 7 and 13. This gives

$$\frac{\mathrm{d}}{\mathrm{d}t}\rho' = -\left[\varepsilon + \frac{2}{3}c_{\mathrm{ds}}\left(1 - \frac{\rho_{\mathrm{s}}'}{\rho'}\right)\frac{1}{H}\right]U\rho'\,. \qquad (16)$$

The equation for dPE/dt then becomes

$$\begin{aligned}\frac{\mathrm{d}}{\mathrm{d}t}\mathrm{PE} &= \frac{\mathrm{d}}{\mathrm{d}t}\left(\frac{\alpha g\rho' VH}{2}\right) = \frac{\mathrm{d}}{\mathrm{d}t}\left(\frac{\alpha g\rho' V^2}{2\pi R^2}\right) \\ &= \left(\frac{2}{V}\frac{\mathrm{d}}{\mathrm{d}t}V - \frac{2}{R}\frac{\mathrm{d}}{\mathrm{d}t}R + \frac{1}{\rho'}\frac{\mathrm{d}}{\mathrm{d}t}\rho'\right)\mathrm{PE} \\ &= \left[\varepsilon - \frac{2}{R} - \frac{2}{3}c_{\mathrm{ds}}\left(1 - \frac{\rho_{\mathrm{s}}'}{\rho'}\right)\frac{1}{H}\right]U\mathrm{PE}\,.\end{aligned} \qquad (17)$$

For dKE/dt, we can proceed in a similar way after taking the derivative of Eq. 4. This gives

$$\begin{aligned}\frac{\mathrm{d}}{\mathrm{d}t}\mathrm{KE} =&\,\rho U^3\left[\frac{1}{4}\varepsilon V + 2\pi H^3(\varepsilon - 2/R)\right] \\ &+ \rho U\left(\frac{1}{2}V + \frac{4\pi}{3}H^3\right)\frac{\mathrm{d}}{\mathrm{d}t}U\,.\end{aligned} \qquad (18)$$

Substituting the expressions for dPE/dt and dKE/dt from Eqs 17 and 18 into the left-hand side of Eq. 15, we obtain

$$\frac{\mathrm{d}}{\mathrm{d}t}U = \left[\frac{V}{2} + \frac{4\pi H^3}{3}\right]^{-1} \left\{ -\left[\frac{1}{4}\varepsilon V + 2\pi H^3 (\varepsilon - 2/R)\right] U^2 \right.$$
$$+ (2/R - \varepsilon)\frac{\alpha g \rho' V H}{2\rho}$$
$$\left. - \varepsilon \left[\frac{1}{4}V + \frac{2\pi}{3}H^3\right] U^2 - \frac{2}{5}\pi c_{\mathrm{ds}} R^2 U^2 - \pi c_{\mathrm{df}} R H U^2 \right\}. \tag{19}$$

The other governing equations are

$$\frac{\mathrm{d}}{\mathrm{d}t}R = U, \tag{20}$$
$$\frac{\mathrm{d}}{\mathrm{d}t}V = \varepsilon U V, \tag{21}$$
$$\frac{\mathrm{d}}{\mathrm{d}t}\rho' = -\left(\varepsilon + \frac{2}{3}c_{\mathrm{ds}}(1 - \rho_s'/\rho')\frac{1}{H}\right) U \rho', \tag{22}$$
$$H = V/(\pi R^2). \tag{23}$$

5 Simplified governing equations

Although Eqs 19-23 form a complete set of governing equations for the uniform, cylindrical cold pool, they are too complicated to provide much insight. Fortunately, many of the terms can be dropped because they are negligible in magnitude. To find out which terms can be dropped, we first need to find the minimum height of the cold pool.

Note that Eqs 21 and 23 can be combined to give

$$\frac{\mathrm{d}}{\mathrm{d}R}H = (\varepsilon - 2/R)H, \tag{24}$$

which, assuming a constant ε, integrates to

$$H = H_0 \left(\frac{R_0}{R}\right)^2 \exp\left[\varepsilon(R - R_0)\right], \tag{25}$$

where R_0 and H_0 are the initial radius and height, respectively. The minimum value of H occurs where $\mathrm{d}H/\mathrm{d}R = 0$, which, according to Eq. 24, is when $R = 2/\varepsilon$. As we will see in section 9, a typical value for the fractional entrainment rate is $\varepsilon = 0.2\ \mathrm{km}^{-1}$. Therefore, the minimum H occurs around $R = 10$ km. Assuming R_0=H_0=1 km, Eq. 25 gives a minimum H of 60 m.

Now, let us turn our attention to the governing equation for ρ', which can be written as

$$\frac{\mathrm{d}}{\mathrm{d}R}\rho' = -\left(\varepsilon + \frac{2c_{\mathrm{ds}}}{3H} + \frac{2c_{\mathrm{ds}}}{3H}\frac{|\rho'_{\mathrm{s}}|}{\rho'}\right)\rho', \tag{26}$$

where we have assumed that $\rho'_{\mathrm{s}} < 0$, meaning that the virtual potential temperature flux off the surface is positive. Assuming that $\varepsilon = 0.2\ \mathrm{km}^{-1}$ and c_{ds}=1.5×10^{-3}, $2c_{\mathrm{ds}}/3H$ is equal to or larger than ε only if $H < 5$ m. As we just learned, however, H never gets smaller than about 60 m, which is an order of magnitude larger than this threshold. Therefore, the second term in parentheses can be dropped. Note that we cannot drop the last term because ρ' can become very small compared with $|\rho'_{\mathrm{s}}|$. After dropping the $2c_{\mathrm{ds}}/3H$ term, we can then use Eq. 25 to replace H in Eq. 26 and then we can integrate, yielding

$$\rho' = \mathrm{e}^{-\varepsilon(R-R_0)}\left[\rho'_0 + \frac{2}{9}c_{\mathrm{ds}}\rho'_{\mathrm{s}}\frac{1}{R_0^2 H_0}\left(R^3 - R_0^3\right)\right]. \tag{27}$$

Note that this is an analytical expression for ρ' as a function of R.

Next, we need to simplify Eq. 19, which is the governing equation for U. First, we will set the form drag coefficient c_{df} to zero; this will be justified in section 9. Second, we will discard all of the H^3 terms. The H^3 terms all stem from the contribution of vertical momentum to the cold pool's kinetic energy. Intuitively, we know that the contribution of vertical momentum to the kinetic energy of a cylindrical cold pool is only relevant in the initial stages as it begins to fall, as some of the potential energy gets briefly routed through vertical kinetic energy on its way to becoming horizontal kinetic energy. Indeed, all of the H^3 terms in Eq. 19 are added to V terms and ,

which decreases rapidly in the initial stages of a cold pool. So, we throw away all of the H^3 terms; this is tantamount to writing

$$\mathrm{KE} = \rho V \frac{1}{4} U^2 \tag{28}$$

rather than the full expression in Eq. 4. Of course, throwing away the H^3 terms adds some error to the initial development of our theoretical cold pool. If we were interested in studying the initial stages of cold pools—say, for R in the range of R_0 to $2R_0$—then this could be a problem. However, our focus here is on the lifetimes and eventual sizes of cold pools, not the initial stages of cold pools, so this approach will suit us fine. In addition, this approximation overestimates the radial kinetic energy only for , which occupies an exceedingly small fraction of the cold

pool's lifetime and maximum area: only ∼6 min of a lifetime that is measured in hours and only ∼1% of the cold pool's eventual area.

At this point, the governing equation for U has been simplified to

$$\frac{\mathrm{d}}{\mathrm{d}t}U = \underbrace{-\varepsilon U^2}_{\text{entrainment drag}} \underbrace{+\left(\frac{2}{R}-\varepsilon\right)\frac{\alpha g \rho' H}{\rho}}_{\text{descent and puffing}} \underbrace{-\frac{4c_{\mathrm{ds}}}{5H}U^2}_{\text{surface drag}} . \tag{29}$$

On the right-hand side, there are three sources and sinks of U, which are due to entrainment drag, exchange of energy between PE and KE, and surface drag. As discussed above, H never becomes small enough for c_{ds}/H to approach the magnitude of ε, so we may discard the third term on the right-hand side. The middle term, however, requires more thought. The piece proportional to $2/R$ is the force that accelerates the cold pool by converting gravitational potential energy to kinetic energy: cold-pool spreading leads to descent that lowers its centre of mass. The piece proportional to ε is a force that decelerates the cold pool by converting kinetic energy to potential energy: cold-pool entrainment causes the cold pool to puff up and raise its centre of mass. For $R < 2/\varepsilon$, the centre of mass descends with time, accelerating the cold pool. For $R > 2/\varepsilon$, the centre of mass ascends with time, decelerating the cold pool. This is something of a strange notion: for $R > 2\varepsilon$, expansion of the cold pool saps it of kinetic energy. As we will see in section 9, the LES cold pools have an entrainment rate that tends to decrease at large R in a way that keeps ε equal to or less than $2/R$, so this behaviour is largely avoided.

Qualitatively, the middle term on the right-hand side of Eq. 29 has its biggest moment at the very beginning of the cold pool's life. In the short time that it takes for the cold pool to increase its radius from R_0 to $2R_0$, about 75% of the initial potential energy is expended. For a cold pool with R_0=H_0=1 km and a 1 K temperature anomaly, this only takes about 6 min. Therefore, rather than try to model the detailed interactions between PE and KE, we will simply put all of the initial PE into KE at the very start. This allows us to drop the middle term on the right-hand side of Eq. 29. By Eqs 12 and 28, we must give the cold pool an initial U equal to

$$U_0 = \sqrt{\frac{2\alpha g \rho_0' H_0}{\rho}} \,. \tag{30}$$

With the understanding that U is to be set to U_0 as given by Eq. 30 at time t = 0, we now have

Integrating, again assuming a constant ε, we obtain

$$U = U_0 \exp\left[-\varepsilon (R - R_0) \right], \tag{31}$$

which is an analytical expression for U as a function of R. Note that this describes a very simple process: the reduction of kinetic energy by entrainment.

Since this is a very simple equation, it can be written in many convenient forms. For example, we can solve for time t as a function of cold-pool radius R,

$$t = \frac{1}{\varepsilon U_0} \left(\exp\left[\varepsilon (R - R_0) \right] - 1 \right) . \tag{32}$$

We can also write down an expression for $R(t)$,

$$R = R_0 + \frac{1}{\varepsilon}\log(1 + t\varepsilon U_0)\,, \tag{33}$$

and an expression for $U(t)$,

$$U = \frac{U_0}{1 + t\varepsilon U_0}\,. \tag{34}$$

Although there are many such equations that can be written down, the simplified theory for a cylindrical cold pool can be completely and succinctly described by the following three equations:

$$R(t) = R_0 + \frac{1}{\varepsilon}\log(1 + t\varepsilon U_0), \tag{35}$$

$$H(R) = H_0\left(\frac{R_0}{R}\right)^2 \exp\left[\varepsilon(R - R_0)\right], \tag{36}$$

$$\rho'(R) = e^{-\varepsilon(R-R_0)}\left(\rho_0' + \frac{2}{9}c_{ds}\rho_s'\frac{1}{R_0^2 H_0}(R^3 - R_0^3)\right)\,. \tag{37}$$

6 Radius and time of death

These equations can be used to predict the demise of cold pools. Let us define the termination—or, more colloquially, the death—of a cold pool as the time when it ceases to be cold. To acknowledge the virtual-temperature effect of water vapour, we can be more precise by defining the termination of a cold pool as the time when ρ'=0. Note that we will be using the equations derived in the previous section, which apply to an isolated cold pool over a flat surface with no mean wind; a mean wind, topography, or collisions with other cold pools could all hasten a cold pool's demise. Throughout the article, we will denote the terminal time and terminal radius as $t_{\rho'=0}$ and $R_{\rho'=0}$, respectively.

We can solve for the terminal radius by setting ρ'=0 in 37. This gives

$$R_{\rho'=0} = R_0 \left(1 + \frac{9}{2c_{\mathrm{ds}}} \frac{H_0}{R_0} \frac{\rho'_0}{|\rho'_{\mathrm{s}}|}\right)^{1/3} , \quad (38)$$

which, surprisingly, has no dependence on the entrainment rate. Note that, for c_{ds}=1.5 × 10^{-3}, $9/2c_{ds}$ equals 3000. Therefore, so long as $R_0|\rho'_s|$ is not three orders of magnitude larger than $H_0\rho'_0$, the terminal R is very well approximated by the second term in parentheses. In fact, inspection of cold-pool transects from LES of radiative–convective equilibrium (Jeevanjee and Romps, 2015) reveals that $H_0/R_0\sim 1$ and $\rho'_0/|\rho'_s|\sim 1$. Therefore, we can safely simplify this expression to

$$R_{\rho'=0} = R_0 \left(\frac{9}{2c_{\mathrm{ds}}} \frac{H_0}{R_0} \frac{\rho'_0}{|\rho'_{\mathrm{s}}|}\right)^{1/3} . \quad (39)$$

Due to the 1/3 exponent, the dependence of $R_{\rho'=0}$ on H_0/R_0 and $\rho'_0/|\rho'_s|$ is weak. If we take $H_0/R_0\approx 1$ and $\rho'_0/|\rho'_s|\approx 1$, then

$$R_{\rho'=0} \approx R_0 \left(\frac{9}{2c_{\mathrm{ds}}}\right)^{1/3} = 14 R_0 . \quad (40)$$

Therefore, from pure physical reasoning, we can conclude that the terminal radius of a cold pool is about 14 times its initial radius. Figure 1 shows the dependence of $R_{\rho'=0}/R_0$ as a function of $H_0\rho'_0/R_0|\rho'_s|$. Thanks to the 1/3 exponent in Eq. 38, the terminal radius varies over a small range (7–31 km) even as $H_0\rho'_0/R_0|\rho'_s|$ is varied over two orders of magnitude (from 0.1–10).

Using $R = R_{\rho'=0}$ in Eq. 32 gives the time when the cold pool ceases to be cold:

$$t_{\rho'=0} = \frac{1}{\varepsilon U_0} \left(\exp\left[\varepsilon (R_{\rho'=0} - R_0)\right] - 1\right) . \quad (41)$$

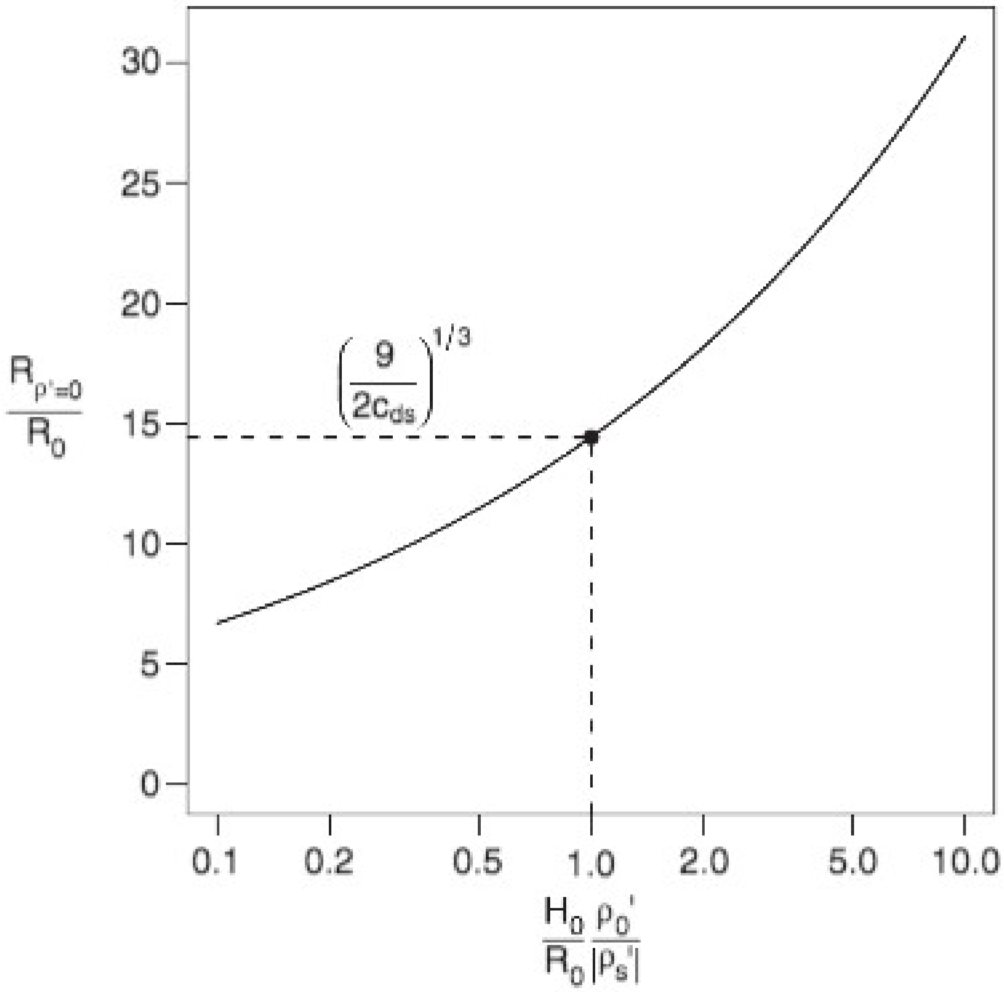

Figure 1. The terminal radius $R_{\rho'=0}$ from Eq. (38) plotted as a function of $H_0\rho_0'/R_0|\rho_s'|$. Thanks to the 1/3 exponent in Eq. (38), $R_{\rho'=0}$ ranges only over a factor of 4, as $H_0\rho_0'/R_0|\rho_s'|$ varies over a factor of 100. The dashed lines denote the values of $H_0\rho_0'/R_0|\rho_s'| = 1$ and $R_{\rho'=0}/R_0 = 14$ from Eq. (40).

While the terminal radius of a cold pool is constrained to lie within roughly a factor of 2 of $14R_0$, the terminal time can vary over a much larger range. This occurs because, in the expression for $t_{\rho'=0}$, there is both a factor of $1/U_0$ and an exponential of $R_{\rho'=0}$. Note that the terminal radius does not depend on U_0 because the two processes that reduce ρ'—entrainment and surface fluxes—operate on a per-distance fashion. Therefore, a halving of U_0leaves the terminal radius unchanged, but it doubles the terminal time. The sensitivity of $t_{\rho'=0}$ is illustrated in Figure 2, which shows $R_{\rho'=0}$ and $t_{\rho'=0}$ as heat maps plotted on axes of $H_0\rho'_0/R_0|\rho'_s|$ and $gH_0\rho'_0/\rho$, assuming R_0=1 km and ε = 0.2 km^{-1}. Both axes are chosen to range over two orders of magnitude, centred on the values obtained using R_0=H_0=1 km and ρ'_0=$|\rho'_s|$=1 K. As in Figure 1, $R_{\rho'=0}$ varies by only a factor of 4 from its lowest value to its highest value (i.e. within a factor of 2 of 14 km). In contrast, $t_{\rho'=0}$ varies over a range covering more than three orders of magnitude, from about 10 min to 10 days.

Figure 2
Open in figure viewerPowerPoint
(a) The terminal radius $R_{\rho'=0}$ given by Eq. 38, plotted as a function of $H_0\rho'_0/R_0|\rho'_s|$ and $gH_0\rho'_0/\rho$ for R_0=1 km and ε = 0.2 km^{-1}. Note that $R_{\rho'=0}$ depends only on $H_0\rho'_0/R_0|\rho'_s|$ and varies only over a factor of 4 for a factor-of-100 range in $H_0\rho'_0/R_0|\rho'_s|$. (b) The same, but for the terminal time $t_{\rho'=0}$ obtained from Eq. 41. Unlike the terminal radius, the terminal time depends on both expressions and it ranges here over three orders of magnitude. The circles denote the locations in parameter space of the large-eddy simulations presented in section 8.
Caption

Since Eq. 38 has no dependence on ε, it is tempting to think that entrainment plays no role in setting the terminal radius. On the contrary, entrainment plays a very important role in setting $R_{\rho'=0}$. In the derivation of Eq. 26 for ρ', entrainment allowed us to neglect the piece of the surface flux that scales as ρ' (this was the argument about H having a finite lower bound). Why were we able to neglect this term? After all, the surface enthalpy flux is proportional to $\rho'-\rho'_s$, so it might seem odd that we could neglect the ρ' part of this. The reason, though, is simple. Entrainment quickly reduces ρ' towards zero and it does so without changing the total mass anomaly $V\rho'$. As a result, entrainment 'hides' the coldness of the cold pool from the surface without changing the total amount of enthalpy needed from the surface to terminate the cold pool, which is proportional to the mass anomaly $V\rho'$. Therefore entrainment plays a vital role in generating Eq. 38 even though it does not show up explicitly there.

In fact, we can see this mechanism at work in Eq. 39. Noting that the initial cold-pool volume V_0 is equal to , we can write 39 as

(42)

$$R_{\rho'=0} = \left(\frac{9V_0\rho'_0}{2\pi c_{\mathrm{ds}}|\rho'_s|}\right)^{1/3} .$$

In the numerator, $V_0\rho'_0$ is the cold pool's initial mass anomaly, which can only be reduced by surface fluxes. Since entrainment quickly hides the coldness of the cold pool (i.e.), $|\rho'_s|$ is

the density difference between the cold pool and the air in direct contact with the surface. Therefore, $c_d|\rho'_s|$ in the denominator is proportional to the surface enthalpy flux. The cube root is explained by the fact that the integrated surface flux is proportional to the product of the cold-pool surface area (order R^2) and the total translation of the cold pool over the surface (order R).

To quantify the effect of entrainment on $R_{\rho'=0}$, we can recalculate the expression for $R_{\rho'=0}$assuming zero entrainment. To do this, we need to start over from Eq. 26, set $\varepsilon = 0$ and retain the $c_{ds}\rho'$ term. The resulting expression is

$$R_{\rho'=0} = R_0\left[1+\frac{9}{2c_d}\frac{H_0}{R_0}\log\left(1+\frac{\rho'_0}{|\rho'_s|}\right)\right]^{1/3} \qquad (\text{for } \varepsilon = 0)\,. \tag{43}$$

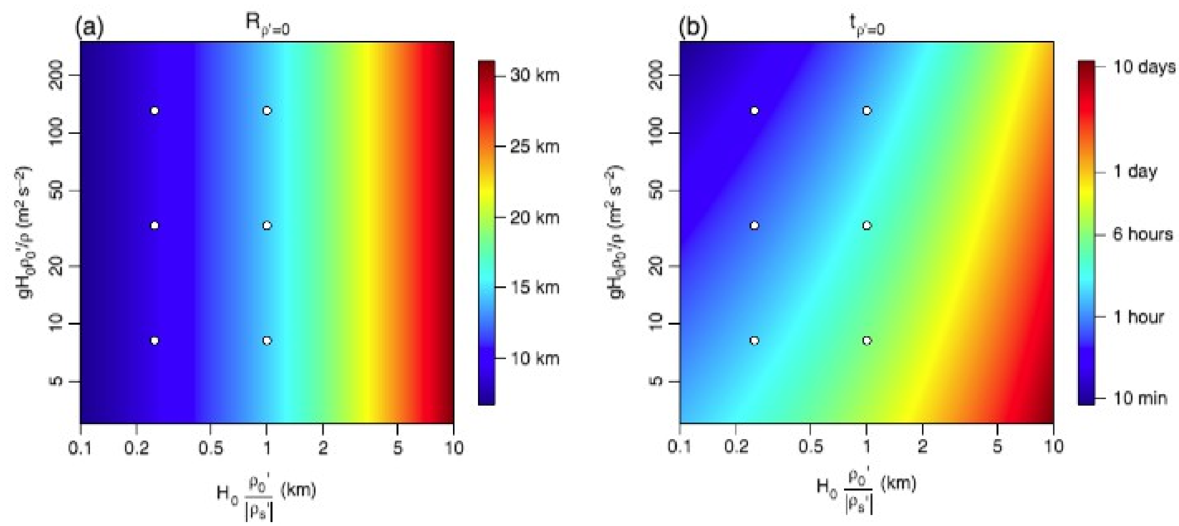

This is practically the same as Eq. 13 of Ross *et al.* (2004), who derived a box model for cold pools by ignoring entrainment entirely. The one difference is the factor of 9/2 here, which is 3 in Ross *et al.* (2004), stemming from the mistake of using $u^r=U$ rather than $u^r=Ur/R$. For small $\rho'_0/|\rho'_s|$, Eq. 43 simplifies to Eq. 38. For large $\rho'_0/|\rho'_s|$, however, Eqs 43 and 38 differ substantially. If a cold pool with $R_0=H_0=1$ km is 2 K colder than its surroundings and if the ambient air–sea temperature difference is 0.2 K, then $\rho'_0/|\rho'_s|$ equals 10. In this case, Eq. 38predicts $R_{\rho'=0}$=31 km while Eq. 43 predicts $R_{\rho'=0}$=19 km. By hiding the cold pool's total thermal deficit (equivalently, its $\rho' V$), entrainment reduces surface fluxes and increases the terminal sizes of cold pools.

Before concluding this section, let us consider whether the initial condition assumed here—a static cylinder of cold air—is appropriate and generalizable to more realistic conditions. In a real rain event, there is a finite time during which cold air is generated and fed into the cold pool. Given a typical updraught speed of 10 m s^{-1} and an atmospheric scale height of 10 km, we might expect the duration of precipitation shafts to be about 10 km/10 m s^{-1}≈20 min. Indeed, this is the typical lifetime of precipitation shafts in the large-eddy simulations of radiative–convective equilibrium performed by Jeevanjee and Romps (2015). Since 20 min is short compared with the lifetimes of cold pools predicted here, the use of instantaneously generated cold pools is appropriate.

To apply Eqs 41 and 42 to cold pools that are measured in observations or LES, we must generalize the definitions of R_0, V_0, ρ'_0, and U_0 to those cases. For R_0, this is straightforward: we can define R_0 as the halfwidth of the precipitation shaft or, for non-circular rain footprints, we can define R_0 as the square root of the footprint divided by π. For V_0, U_0, and ρ'_0, we can calculate these variables based on the air that flows laterally out of the rain shaft. For notational simplicity, imagine that the rain shaft has a circular footprint of radius R_0. Then the total initial cold-pool mass ($\rho_0 V_0$), mass anomaly ($\rho'_0 V_0$), and kinetic energy ( ) are given by

$$\rho_0 V_0 = R_0 \int_0^T \mathrm{d}t \int_0^{2\pi} \mathrm{d}\phi \int_0^{z_{\mathrm{BL}}} u^r \mathcal{H}(u^r) \rho \, \mathrm{d}z, \qquad (44)$$

$$\rho'_0 V_0 = R_0 \int_0^T \mathrm{d}t \int_0^{2\pi} \mathrm{d}\phi \int_0^{z_{\mathrm{BL}}} u^r \mathcal{H}(u^r) \rho' \, \mathrm{d}z, \qquad (45)$$

$$\rho_0 V_0 \frac{1}{4} U_0^2 = R_0 \int_0^T \mathrm{d}t \int_0^{2\pi} \mathrm{d}\phi \times \int_0^{z_{\mathrm{BL}}} u^r \mathcal{H}(u^r) \left[\rho' g z + \frac{1}{2} \rho u^{r2} + \frac{1}{2} \rho w^2 \right] \mathrm{d}z\,, \qquad (46)$$

where z_{BL} is the depth of the boundary layer, ρ_0 is the density of boundary-layer air, φ is the azimuth about the cold-pool centre, T is the duration of the precipitation shaft, and is the

Heaviside unit step function. After solving these equations for V_0, U_0, and ρ'_0, the results can be plugged into Eqs 41 and 42 to estimate the terminal time and radius.

7 Measuring in LES

To evaluate this theory, we will use large-eddy simulations of individual cold pools initialized as cold cylinders of air. To keep track of a cold pool's evolution, we will use a passive tracer, the mixing ratio of which is initialized to one within the initial cold pool and zero outside. As in Romps and Kuang (2010), we will refer to this as the purity tracer. Since cold pools in LES do not retain a uniform, cylindrical shape, we must make some choices about how to calculate the cold pool's volume, radius, and density anomaly.

Let us define

where q is the purity mixing ratio and X is one of the following: 1, q, u, v, and ρ'. Here, u and $v$are the horizontal wind components and $\rho'=\rho(x,y,z,t) - \rho_{env}(z,t = 0)$, where $\rho_{env}(z,t = 0)$ is the initial profile of density in the environment. In all of the LES, the instantaneous two-dimensional distributions of these quantities are saved every 2 min. From these quantities, we can define a cold-pool height distribution $h(x,y,t)$, total mass $M(t)$, radial-velocity distribution $u^r(x,y,t)$, density-anomaly distribution $\rho'(x,y,t)$, mean density anomaly $\rho'(t)$, and radius $R(t)$. To find the correct expressions for these variables, we will find the expressions that give the correct answers for a uniform cylinder. For a cylinder with uniform density ρ, uniform purity q, and depth h,

From this equation, we can see, for example, that $\langle 1\rangle^2/\rho\langle q\rangle$ equals the cold pool's height h. Therefore, for the LES output, we define the cold-pool height $h(x,y,t)$ as

$$h(x,y,t) = \frac{\langle 1\rangle^2}{\rho\langle q\rangle}, \tag{47}$$

where ρ is a constant representative density near the surface, and we define the total mass of the cold pool as

$$M(t) = \int_A \frac{\langle 1 \rangle^2}{\langle q \rangle} \, \mathrm{d}^2 x \,, \tag{48}$$

where A is the area over which $\langle q \rangle$ is above some threshold value (we use 0.01 kg m^{-2}). Proceeding in the same way, we find that $u^r(x,y,t)$, $\rho'(x,y,t)$, and $\rho'(t)$ should be defined as

$$u^r(x,y,t) = \frac{\langle u \rangle x + \langle v \rangle y}{\langle 1 \rangle \sqrt{x^2 + y^2}}, \tag{49}$$

$$\rho'(x,y,t) = \frac{\langle \rho' \rangle}{\langle 1 \rangle}, \tag{50}$$

$$\rho'(t) = \frac{1}{M} \int_A \frac{\langle \rho' \rangle \langle 1 \rangle}{\langle q \rangle} \, \mathrm{d}^2 x \,. \tag{51}$$

To borrow a phrase from computer science, we are ‘overloading’ the symbol ρ' to mean different things in different contexts in order to simplify the notation. When ρ' refers to a four-dimensional variable, it equals $\rho(x,y,z,t) - \rho_{\mathrm{env}}(z,t = 0)$. When ρ' refers to a three-dimensional variable, it is given by Eq. 50. When ρ' refers to a one-dimensional variable, it is given by Eq. 51. In the text and figures that follow, context will make clear which definition is being used.

We define the cold-pool radius $R(t)$ somewhat differently, so that it captures the location of the cold-pool front as accurately as possible. For a uniform cylinder, the radius R can be written as the following integral for any $n \geq 1$:

$$R = \frac{n+1}{n} \frac{\int_A \langle 1 \rangle r^{n-1} \, \mathrm{d}^2 x}{\int_A \langle 1 \rangle r^{n-2} \, \mathrm{d}^2 x} \,. \tag{52}$$

For a non-uniform cold pool, this will give the distance from the centre to the edge that is farthest away in the limit of . Since this limit is noisy, we use $n = 10$, which gives an

accurate and smooth $R(t)$. The radius obtained in this way is very similar to the one obtained by taking the square root of the area of $\langle q \rangle > 0.01$ divided by π. Finally, we diagnose the fractional entrainment rate ε as

$$\varepsilon = \frac{\mathrm{d}}{\mathrm{d}R} \log(M) \,. \tag{53}$$

8 The large-eddy simulations

Table 1 describes the nine LES that are used for comparison with the theory developed in the previous sections. All of the simulations were initialized with a motionless, cylindrical cold pool with a uniform temperature perturbation defined relative to the environment at the same height. For computational feasibility, all of the cold pools have an initial height H_0 and initial radius R_0 equal to one kilometre; larger initial heights and radii would have required larger computational domains. Both the cold pool and the environment are dry and have a dry-adiabatic lapse rate. A small amount of random noise is added to the initial temperature field to break the symmetry. For each of the nine simulations, Table 1 specifies whether or not surface fluxes of momentum (i.e. drag) or enthalpy are communicated between the surface and the atmosphere. In either case, the fluxes are calculated using the bulk aerodynamic formula, i.e. $-c_{ds}\rho|\mathbf{u}|\mathbf{u}$ or $c_{ds}\rho|\mathbf{u}|(T_{surf}-T)$, with a drag coefficient $c_{ds}=1.5 \times 10^{-3}$. The temperatures in Table 1 specify the initial cold-pool surface air temperature T_{cp}, the initial environmental surface air temperature T_{env}, and the surface temperature T_{surf}. The identifying numbers (i.e. 1–9) assigned to each simulation in Table 1 will be used throughout the article.

Table 1. A list of the large-eddy simulations indicating whether or not surface drag was present, whether or not surface enthalpy fluxes were present, the temperature of the cold pool T_{cp}, the temperature of the environmental surface air T_{env}, and the temperature of the sea-surface T_{surf}.

LES #	Surface drag?	Enthalpy fluxes?	T_{cp} (K)	T_{env} (K)	T_{surf} (K)
1	No	No	299	300	301
2	No	Yes	299	300	301
3	Yes	No	299	300	301
4	Yes	Yes	299	300	301
5	Yes	Yes	299	300	304
6	Yes	Yes	299.75	300	301
7	Yes	Yes	296	300	304
8	Yes	Yes	296	300	316
9	Yes	Yes	299.75	300	300.25

All of the LES are performed using Das Atmosphärische Modell (DAM: Romps, 2008), which is a fully compressible large-eddy model. All of the simulations are performed without radiation, without microphysics (all of the simulations are dry), and without planetary rotation. The domains have a model top at 3 km and a square horizontal domain that is sufficiently large to encompass the cold pool throughout the 3.5 h of simulation (38.4 km square for all of the simulations). The horizontal grid spacing is $\Delta x = \Delta y = 50$ m and the vertical grid spacing is $\Delta z = 10$ m for $z < 600$ m, $\Delta z = 50$ m for $z > 1300$ m, and smoothly transitioning in between.

9 Comparing LES and theory

Our objective in this section is to compare the cold-pool theory with the large-eddy simulations of cold pools. Before we can do that, however, we must use the LES to find the appropriate values of α (the fraction of gravitational energy converted to cold-pool kinetic energy) and c_{df} (the form-drag coefficient). For this purpose, we use LES 1 and our full theoretical equations 19-23 to find the best choice of α and c_{df}. We use LES 1 for this exercise because it is the simplest of all the LES, in the sense that it has neither surface drag nor enthalpy fluxes; including those surface fluxes would only increase the sources of potential error in the theoretical calculation and therefore add error to the calculated best-fitting α and c_{df}. Also, to reduce the treatment of entrainment as a potential source of error, we give the theoretical equations the actual $\epsilon(R)$ diagnosed from the LES.

Figure 3 plots the root-mean-square difference between $R(t)$ calculated from Eqs 19-23 and $R(t)$ calculated from Eq. 52. The best fits are obtained for c_{df}=0, indicating that form drag is negligible. This is an interesting result, especially in comparison with recent findings that cloud thermals experience significant drag (Romps and Charn, 2015), despite having, like cold pools, an internal vortex-ring circulation. These results are not inconsistent, because wave drag was identified as a likely dominant source of drag for cloud thermals (Romps and Öktem, 2015), whereas there is no wave drag in these simulations with neutral stratification. (Waves can be supported on the interface between the cold pool and the environment, but there is no way for those waves to propagate away from the cold pool and therefore no way for them to remove momentum from the cold pool.) Also, it is important to note that the entrainment drag is calculated as if the entrained air has zero momentum, which may overestimate the entrainment drag and therefore give a best fit with a less-than-realistic c_{df}. As for α, although it is difficult to tell from Figure 3, the best fit occurs for a value of 0.7. In other words, 70% of the cold pool's gravitational potential energy is converted to kinetic energy of the cold pool, with the remainder going into the kinetic energy of the environment. These values of c_{df}=0 and $\alpha = 0.7$ will be used in all theoretical calculations henceforth.

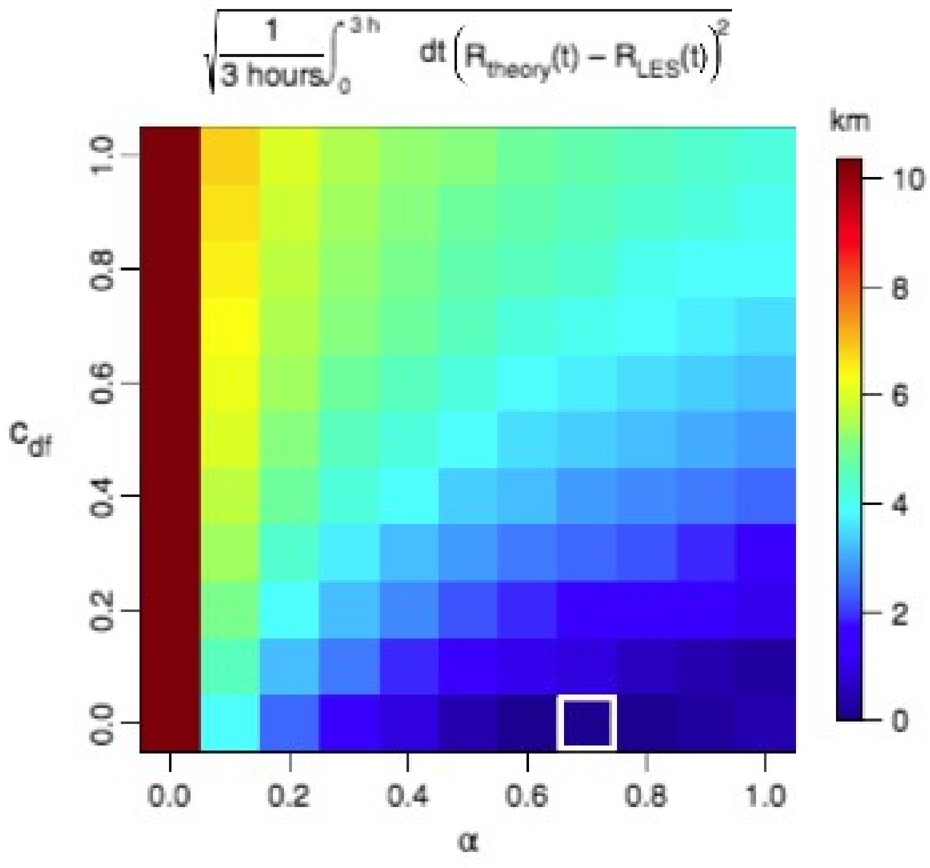

Figure 3

For LES 1 (no surface fluxes of momentum or enthalpy and an initial 299/300/301 K temperature distribution), the 3 h root-mean-square difference between the $R(t)$ diagnosed from the LES and the $R(t)$ governed by Eqs 19-23 for different values of (abscissa) α and (ordinate) c_{df}. The best fit occurs for c_{df}=0 and α = 0.7, which is highlighted with a white box; these values are used in all subsequent figures.

Figure 4(a) shows that the theoretical solution for $R(t)$ using the full theory with $\varepsilon(R)$ diagnosed from the LES is indeed a good fit to the LES. However, in order to use the simplified equations derived in section 5, we must pick a constant fractional entrainment rate. Figure 4(b) shows that the full theory—i.e. Eqs 19-23 from section 4—with a constant fractional entrainment rate of ε = 0.2 km^{-1} is also a good fit to the LES. For comparison, the solutions with ε = 0.1 and 0.3 km^{-1} are shown; these are poor fits. Next, we can evaluate the simplified theory—i.e. Eqs 35-37 from section 5—by plotting their $R(t)$ against the $R(t)$ from the full theory. As argued in section 5, the full theory and simplified theory should agree quite well. Indeed, Figure 4(c) confirms this.

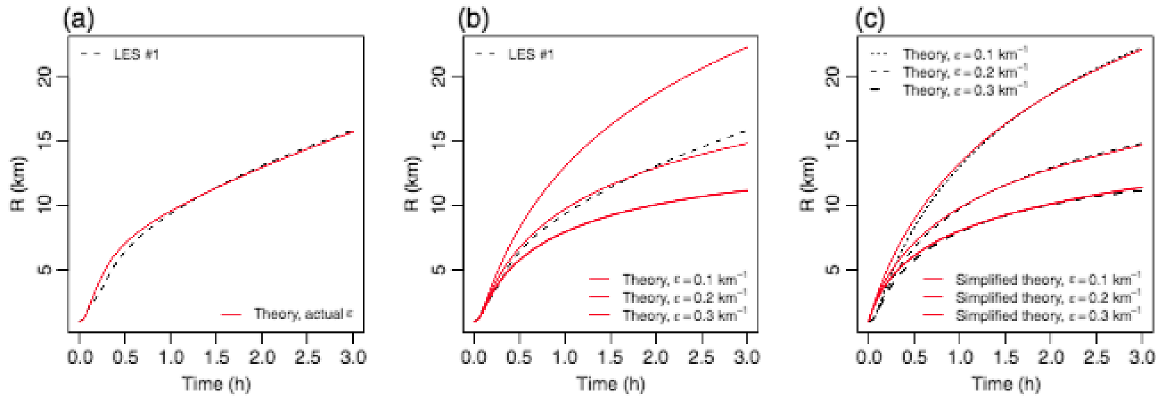

Figure 4

(a) A comparison of $R(t)$ for (dashed black) LES 1 and (solid red) the full theory given by Eqs 19-23using the actual $\varepsilon(R)$ diagnosed from the LES. (b) A comparison of $R(t)$ for (dashed black) LES 1 and (solid red) the full theory using a constant ε equal to 0.1, 0.2, and 0.3 km^{-1}. (c) A comparison of (dashed black) the full theory using constant ε and (solid red) the simplified theory given by Eqs 35-37 using the same constant ε. These panels demonstrate that the full numerical theory is an excellent match to the LES and very little error is introduced by assuming a constant entrainment rate or by using the simplified governing equations.

Now, what do these LES and theoretical cold pools look like from a bird's-eye view? To give a sense for this, Figure 5 gives the plan view of $h(x,y,t)$, $u^r(x,y,t)$, and $\rho'(x,y,t)$ (multiplied by $-\rho/T$ to convert it to a temperature perturbation) for LES 4 (arguably, the most realistic of the nine simulations) at 30 min intervals, along with the corresponding simplified theory from Eqs 35-37. Figure 6 plots the same information, but azimuthally averaged at 30 min intervals. Of course, there is a great deal of internal structure to real cold pools that cannot be captured by a uniform cylinder. Nevertheless, the simplified theory does a decent job of capturing the size and horizontally averaged properties of the LES cold pool. Note that, in the azimuthal averages, many of the largest discrepancies between the LES and theory occur at small radii, which make a small contribution to the cold pool's area.

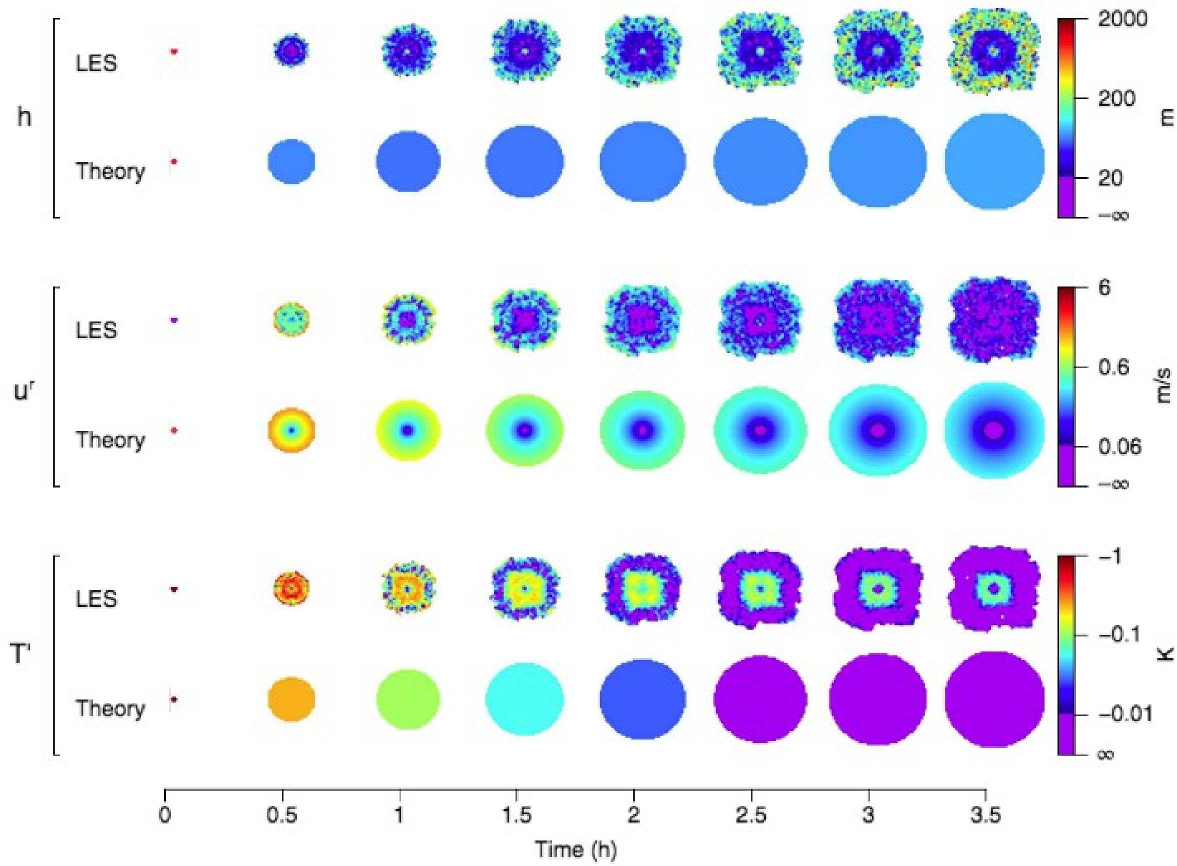

Figure 5

Snapshots of cold-pool properties from LES 4 in Table 3(i.e. with surface enthalpy fluxes, surface drag and an initial 299/300/301 K temperature distribution) and the corresponding theoretical solution using Eq. 36 for h, Eqs 2 and 31 for u^r and Eq. 37 for ρ', which is then multiplied by $-\rho/T$to express it as a temperature perturbation T'.

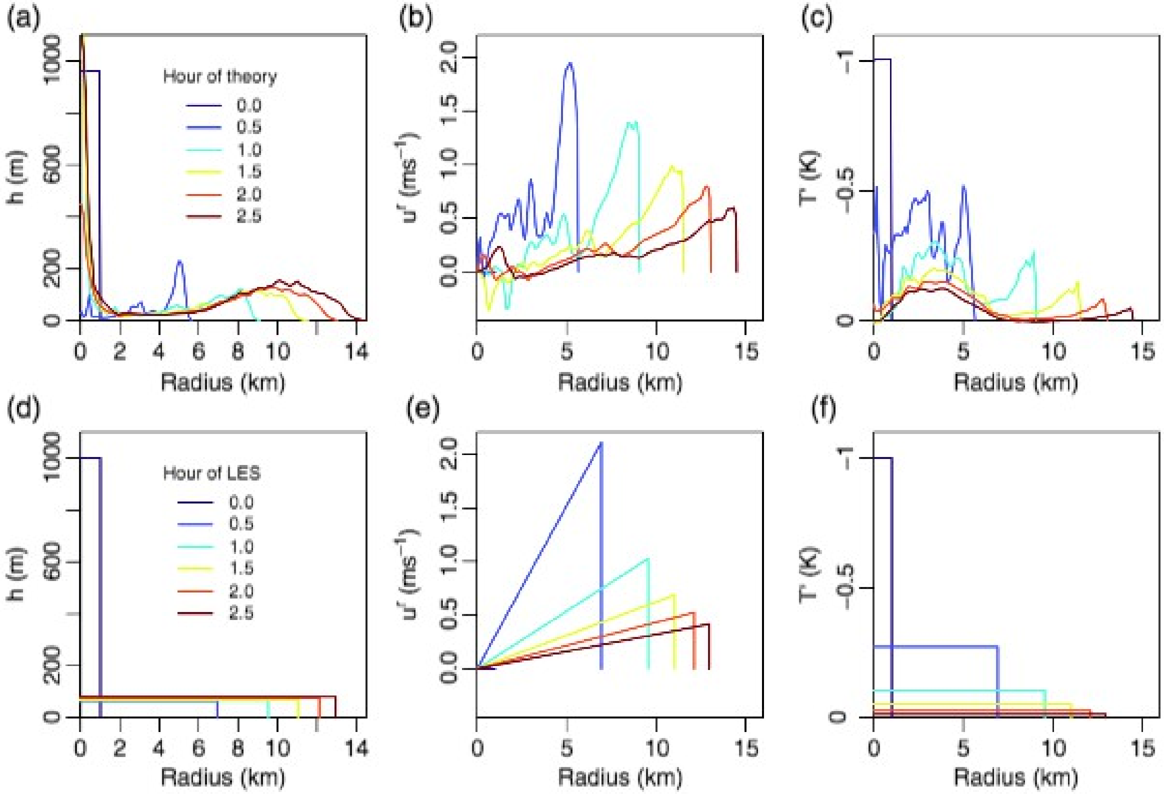

Figure 6

(a)–(c) Azimuthal averages of cold-pool height h, radial velocity u^r and temperature anomaly T' for LES 4 at 30 min intervals and (d)–(f) the same, but from the corresponding theoretical solution using Eq. 36 for h, Eqs 2 and 31 for u^r and Eq. 37 for ρ', which is then multiplied by $-\rho/T$to express it as a temperature perturbation T'.

Caption

A key conclusion from section 5, codified in Eq. 35, is that $R(t)$ is largely insensitive to drag and surface enthalpy fluxes. We can check this by comparing the $R(t)$ from LES 1–4, which share the same initial temperature distribution but differ in whether or not they have surface drag. These $R(t)$ are plotted in Figure 7(a), where $R(t)$ is on the abscissa to be consistent with the other panels. The dashed curves have no surface drag, while the solid curves do. The black curves have no surface enthalpy flux, while the red curves do. The triangles denote where the cold pools terminate (i.e. cease to be cold); trajectories beyond those radii are plotted in pink. All of the cold pools have very similar $R(t)$, in agreement with the theory.

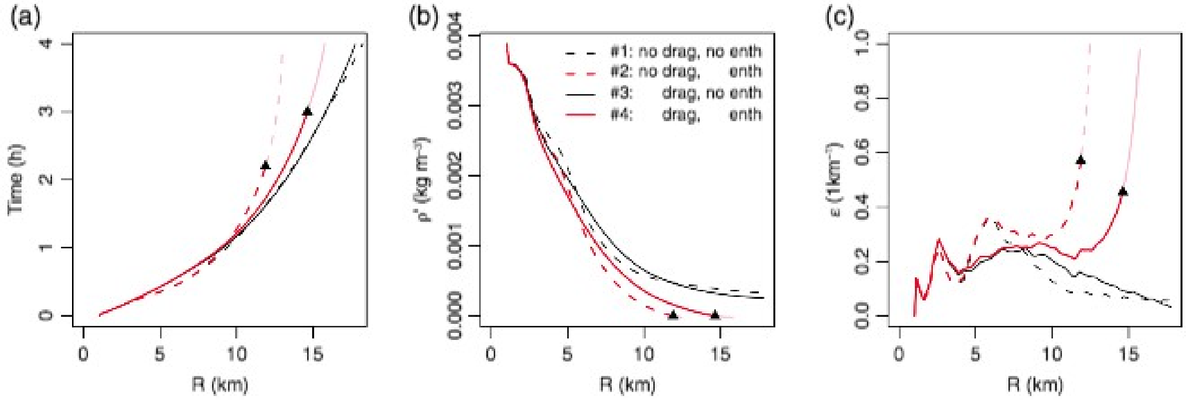

Figure 7
As a function of cold-pool radius *R*, (a) time, (b) cold-pool density anomaly and (c) cold-pool entrainment rate for LES 1–4 in Table 3(i.e. with an initial 299/300/301 K temperature distribution). Simulations with surface enthalpy fluxes are red; those without are black. Simulations with surface drag are solid; those without are dashed. Triangles denote where the cold pools cease to be 'cold' pools; curves beyond those points are faded to emphasize that those are no longer cold pools, strictly speaking. In (a), note that the four $R(t)$ curves are very similar, indicating an insensitivity to surface enthalpy and momentum fluxes. In (c), note that the entrainment rates are also very similar, up to the point where cold pools start to have enhanced mixing due to patches of neutrally or positively buoyant air.

Significant deviations from a common $R(t)$ occur only when the cold pools begin to have significant regions of , i.e. as they are dying. This only occurs for the red curves because only those simulations have surface enthalpy fluxes. Figure 7(b) shows the mean ρ' as a function of radius. As the mean ρ' approaches zero, the entrainment rate, shown in Figure 7(c), starts to grow rapidly. This occurs because the stratification between the cold pool and its environment is removed, allowing enhanced mixing by mechanical forcing and even by buoyant convection for regions of the 'cold' pool with $\rho'<0$.

For LES 1 and 3, which have no surface enthalpy fluxes, the total mass anomaly $V\rho'$ does not change in time, so the cold pool remains cold forever. It is intuitive that such a cold pool would continue to spread until it has blanketed the entire domain. Equation 29, however, suggests that this might not happen if ε exceeds $2/R$. As discussed in section 5, this would cause PE to grow as the cold pool expands, which would happen at the expense of KE. If ε remained larger than $2/R$ for long enough, this could grind the cold pool to a halt, leaving untapped PE sitting motionless in the atmosphere. This is an absurd result, so something must prevent this from happening. That 'something' is that ε must decrease with radius to stay roughly at or below a bound of 2/R. This behaviour can be seen in the black curves in Figure 7(c). At about 7 km, 2/Rbecomes small enough to equal ε, but ε decreases to stay at or under the 2/R bound for all $R >$ 7 km.

Another set of key theoretical predictions consists of Eqs 38 and 41, which give expressions for the terminal radius $R_{\rho'=0}$ and the terminal time $t_{\rho'=0}$. Figure 8 plots the terminal radius and time from the seven LES with surface enthalpy fluxes against the corresponding predictions from Eqs 38 and 41, respectively. One-to-one lines are added for visual reference. Although not perfect, the simple theory does a good job of predicting the location and timing of cold-pool death.

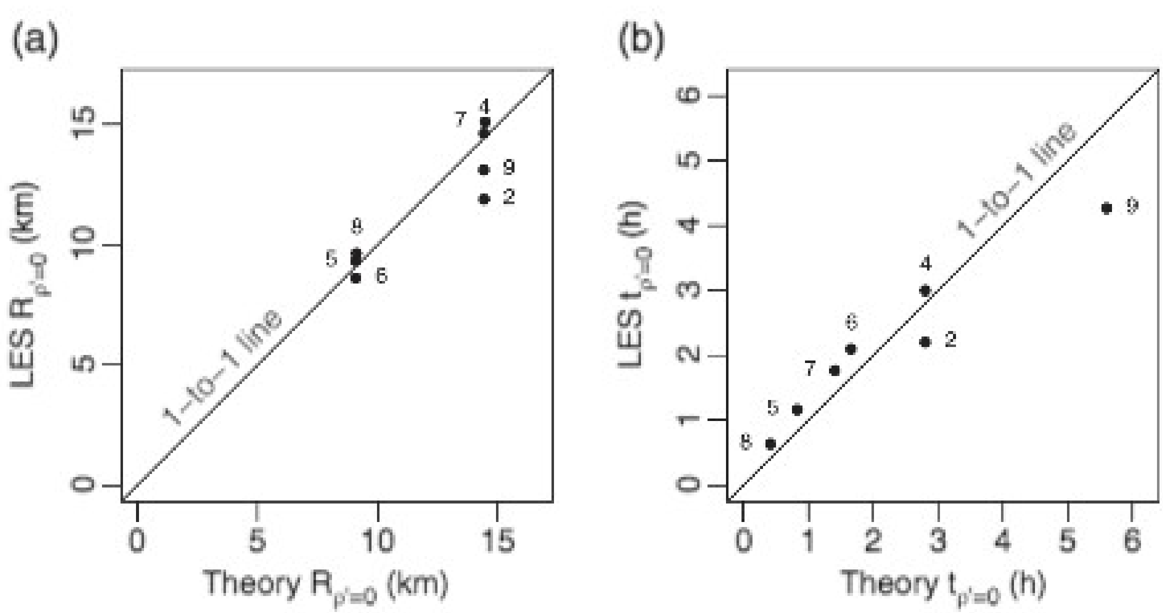

Figure 8
(a) For LES 2 and 4–9, the radii at which the cold pools terminate (i.e. cease to be cold) are plotted against the corresponding theoretical prediction. Note that LES 1 and 3 are not included, because their lack of surface enthalpy fluxes means that they never cease to be cold (i.e. never achieve ρ'=0). (b) The same, but for the time at which the cold pools terminate.
Caption

It is interesting to note that LES 4, which has surface drag, terminates at a *larger* radius and *later* time than LES 2, which is the same in all respects except that it has no surface drag.

This may be counterintuitive, since it is natural to imagine that surface drag would slow down the cold pool, leading to an earlier demise at a smaller radius. On the contrary, the addition of surface drag reduces the low-level wind speed relative to the bulk of the cold pool, thereby reducing the enthalpy fluxes. Since it is the zero crossing of ρ' that terminates a cold pool, surface drag leads to a later termination at a larger radius.

10 Summary and discussion

With the goal of understanding the dynamics of real cold pools, we have derived the governing equations for a uniform, cylindrical cold pool. Inspection of the magnitudes of terms in the equations reveals that the cold-pool dynamics has only a weak dependence on surface drag that can be neglected. With this and some other well-justified approximations, the governing equations reduce to a very simple theory for cold-pool dynamics, given by Eqs 35-37. The cold-pool radius is a function of time that depends only on the initial radius, the initial gravitational potential energy, and the fractional entrainment rate.

These equations make predictions for the lifetime and final size of cold pools, defining the demise of a cold pool as when it ceases to be cold on average. The expressions for those terminal sizes and times are given by Eqs 38 and 41 for an initially stationary cold pool, or by Eqs 41 and 42 for a more realistic cold pool with initial values estimated according to Eqs 44-46. Although entrainment reduces ρ' dramatically, the terminal radius—defined as the cold-pool radius when $\rho'=0$—has no dependence on the entrainment rate. By quickly ‘hiding’ the coldness of the cold pool from the surface, entrainment simplifies the estimation of surface fluxes without affecting the total enthalpy fluxes needed to terminate the cold pool; this leads to a very predictable terminal radius that does not depend on the precise value of the entrainment rate. The equations show that the final radius is tightly constrained to be in the vicinity of $\sim$14 times the initial radius, while the terminal time can range over several orders of magnitude. Comparison with large-eddy simulations, as shown in section 9, validates the simple theory and its predictions for cold-pool sizes and lifetimes.

We can also compare our results with previous studies that have measured the sizes and lifetimes of cold pools. Tompkins (2001) studies cold pools in a large-eddy simulation of tropical unorganized convection and finds the mean maximum radius to be 8.6 km. It is important to note, however, that Tompkins (2001) uses a very different definition of cold-pool radius. Here, we measure the radius as the distance from the centre of the cold pool to the outer perimeter of the original cold-pool air, whether or not it is still ‘cold’; Tompkins (2001) measures the radius from the centre of the cold pool to the perimeter of the currently ‘cold’ air (specifically, air with buoyancy less than −0.005 m s^{-2} or a potential temperature anomaly less than −0.15 K). Feng *et al.* (2015) study cold pools in an LES using a similar definition (with a buoyancy threshold of −0.003 m s^{-2}) and find a similar result: a mean maximum radius of 6.4 km. As seen in Figure 5, the definition of radius used by Tompkins (2001) and Feng *et al.* (2015) gives a maximum radius that is only about half as large as the terminal radius. If we account for this by doubling their reported maximum radii, we infer that they simulated cold pools with mean maximum radii of about 13–17 km. This agrees with the theory presented here, which predicts a ∼14 km terminal radius for a cold pool with an initial radius of 1 km and $H_0\rho'_0/R_0|\rho'_s|\sim 1$.

The theory also agrees well with the reported lifetimes. Tompkins (2001) reports a mean cold-pool lifetime of 2.5 h and a mean initial temperature anomaly of −1 K. Using this temperature anomaly to set ρ', using a fractional entrainment rate of 0.2 km^{-1} (as diagnosed in section 9), and using an initial radius and height of 1 km, Eq. 41 predicts a lifetime of 2.8 h, which is in close agreement with 2.5 h. Feng *et al.* (2015) report a shorter lifetime of 1.2 h, but this agrees, at least qualitatively, with their smaller initial temperature anomaly of −0.5 K (see their figure 6(d)). Changing the temperature anomaly from −1 K to −0.5 K, while holding the other variables constant, reduces the lifetime predicted by Eq. 41 from 2.8 to 2.1 h. Differences in the air–sea temperature difference or in the initial cold-pool height or radius could easily explain the remaining discrepancy.

It is more difficult to observe cold pool sizes in nature and even more difficult to measure their lifetimes. At least anecdotally, it appears that cold pools reach a wider range of sizes over the real tropical oceans than they do in large-eddy simulations of the tropical maritime atmosphere. For example, Black (1978), Zuidema *et al.* (2012), and Feng *et al.* (2015) observe real cold pools over tropical oceans with radii of 50–100, 20–30, and 5–25 km, respectively. As noted in the discussion of Eq. 38, it is difficult to generate a wide range of terminal radii by varying just the normalized height H_0/R_0 or the normalized density anomaly $\rho'_0/|\rho'_s|$, since they contribute to the terminal radius with only one-third power. Instead, the variance in the initial radius in Eq. 38 or initial mass anomaly in Eq. 42 is likely the single largest contributor to the observed variance in the terminal radius. For example, assuming a plausible boundary-layer depth H_0 of 1 km and a plausible ratio of $\rho'_0/|\rho'_s|=1$, Eq. 38 would require an initial radius of R_0=20 km to produce a terminal radius of 100 km. Of course, this does not imply a need for a single cylindrical rain shaft that is 40 km across. By Eq. 42, it would also suffice to have five, nearby, 2 km radius rain shafts of 30 min duration that replenish the air in their boundary-layer volume 20 times during their lifetime, which would be possible with modest radial winds of 10 m s^{-1} at the edge of the rain shafts.

In the study of convection, convective entrainment is often cited as the biggest obstacle to developing advanced theories of convective updraughts (de Rooy *et al.*, 2013). Based on the results shown here, we suspect that cold-pool entrainment may prove to be as thorny an issue for cold pools as convective entrainment has been for convection. The similarities are striking. Consider, for example, that a bulk-plume model treats updraughts as homogeneous at each height and our ‘bulk-pool’ model treats cold pools as homogeneous at each time. Also, as in a bulk-plume model, we have been forced to specify an entrainment rate that is motivated by empiricism rather than theory. Fortunately, a cold pool's terminal radius is independent of the entrainment rate, so the theory presented here for cold-pool sizes is likely to stand the test of time. On the other hand, the equations given here for a cold pool's velocity $U(t)$ and terminal time $t_{\rho'=0}$ are highly dependent on the chosen entrainment rate. Since ε may vary significantly with initial radius or may evolve in important ways at larger radii (as suggested by the black curves in Figure 7(c)), the extrapolation of our results for $U(t)$ and $t_{\rho'=0}$ to cold pools with R_0 much larger than those simulated here is not without risk. To know for sure how well these equations and assumptions apply to larger cold pools, more work is needed on simulating and observing a wide range of cold pool types and on developing theories for cold-pool entrainment.

Acknowledgements

This work was supported by the Scientific Discovery through Advanced Computing (SciDAC) program, funded by the US Department of Energy Office of Advanced Scientific Computing Research and Office of Biological and Environmental Research under Contract No. DE-AC02-05CH11231. This research used computing resources of the National Energy Research Scientific Computing Center (NERSC), which is supported by the Office of Science of the US Department of Energy under Contract DE-AC02-05CH11231, and the Extreme Science and Engineering Discovery Environment (XSEDE), which is supported by National Science Foundation grant number ACI-1053575.